JACS
JOURNAL OF THE AMERICAN CHEMICAL SOCIETY

ARTICLE

pubs.acs.org/JACS

Metal Anion−Alkyl Ammonium Complexes as Direct Write Precursors to Produce Nanopatterns of Metals, Nitrides, Oxides, Sulfides, And Alloys

B. Radha, S. Kiruthika, and G. U. Kulkarni*

Chemistry and Physics of Materials Unit and DST Unit on Nanoscience, Jawaharlal Nehru Centre for Advanced Scientific Research, Jakkur P.O., Bangalore 560064, India

Supporting Information

ABSTRACT: The study explores the possibility of using metal anions complexed with tetraoctylammonium bromide (ToABr) as single-source direct write precursors in e-beam and soft lithography processes to obtain micro- and nanoscale patterns of various metals, i.e., Au, Pd, Pt, Ag, Pb and Cu, as well as of their alloys (AuCu), oxides (Co_3O_4, ZnO), nitrides (CoN, InN, GaN), and sulfides (Ag_2S). The extraction efficiency of ToABr for different metal anions is found to be varied (40−90%), but the obtained precursors are easily processable as they have reasonable solubility in common solvents and are obtainable as smooth films, both being important for high-resolution patterning. The e-resist action of the precursors originates from the extreme e-beam sensitivity of the hydrocarbon chain present in ToABr, while direct micromolding has been possible due to easy flow of the precursor solutions in capillaries. The interaction of the anion and ToABr being mainly electrostatic enables easy removal of the hydrocarbon from patterned regions by thermolysis on a hot plate in the ambient or in controlled atmosphere to form the desired product. This method can be easily generalized.

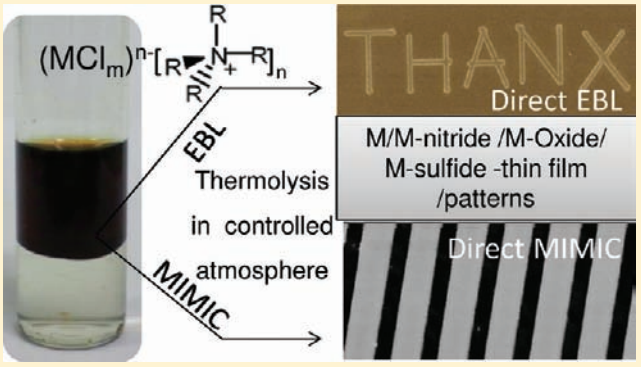

INTRODUCTION

Material applications very often require that a given material with approved properties be cast in the form of a film or a pattern. This requirement in turn demands the most straightforward process recipes involving appropriate chemical precursors.[1] Thus, terms such as single-step process and single-source precursor have become quite popular, nowadays. Drop or spin coating a metal−organic precursor solution and baking under controlled conditions is a common method to produce thin films of the desired material.[2] Direct writing[3] using an energetic electron or ion beam to chemically modify a metal precursor either deposited a priori as a thin film or injected close to the e beam is a well-known method. Writing with an atomic force microscopy (AFM) tip, called dip-pen lithography,[4] or direct imprinting of precursors[5] has also been well established. More than the methods, at present, the quest is around the precursors.[6] Designing and developing precursors suited to processes aimed at producing a given material with prescribed crystallinity, morphology, purity, etc. is a daunting task. A number of precursors have been tried out for varied materials and techniques. For example, starting with metal alkoxide precursors, metal oxide thin-film transistors have been fabricated.[7] Urea complexes have been tried out as single-source precursors for nanostructures of nitrides.[8] Thermal decomposition of metal oleate complexes has been reported for the synthesis of metal and oxide nanocrystals.[9] However, there are no ready solutions to this quest. Here we report how metal anion−alkyl ammonium complexes may be used as single-source direct write precursors in e-beam and soft lithography processes to obtain micro- and nanoscale patterns of various metals as well as of their alloys, oxides, nitrides, and sulfides.

Although the interaction of metal anions with quaternary ammonium salts to form complexes is well-known and widely applied for the extraction of metals from aqueous solutions,[10,11] these complexes had not been commonly employed in materials research. A notable exception has been the Brust method,[12] where $(AuCl_4)^-$ ions extracted using tetraoctylammonium bromide (ToABr) in toluene served as precursors for controlled synthesis of alkanethiol-capped Au nanoparticles in solutions. Since then, colloidal sols of Pt,[13] Pd,[14] Ag,[15] and alloys such as AgAu[16] have been prepared by stabilizing the respective anions with ToABr, thus establishing the usefulness of the ToABr complexes.[17] The method has been varied to obtain various anisotropic nanostructures of Au, Ag, Cu, etc., by playing with the reducing agent.[18] However, these complexes have not been explored as precursors in lithography processes. We realized that the precursors are easily processable as they have reasonable solubility in common solvents and are obtainable as smooth

Received: April 29, 2011
Published: July 26, 2011

Scheme 1. Process Flow for the Preparation of Patterns and Thin Films of Metals and Their Alloys, Metal Nitrides, Oxides, and Sulfides

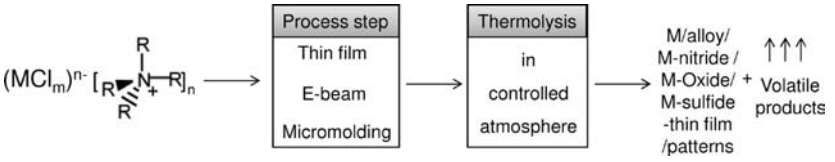

films, both being important for high-resolution patterning. The hydrocarbon part is expected to be highly sensitive to the e-beam[19] and is easily detachable by thermal activation.[20] The liberated anion is reactive to produce the desired end product (Scheme 1).

This scheme of process is essentially direct write lithography which in contrast to conventional lithography methods does not use polymeric resists taken through a number of process steps such as exposure, development, metal deposition, and lift-off or etching; the latter steps although crucial often lead to incorporation of contaminants into the patterned materials. The increasing interest in direct write e-beam lithography (EBL) methods is evident in the recent years. Au nanoparticles capped with alkanethiol ligands[21] and Pd clusters protected by ToABr[22] have served as e-beam resists to write metal nanopatterns. Instead of nanoparticle films, metal−organic precursor films are preferred, as they are relatively more sensitive requiring less e-dosage.[19,23] Using Ni naphthenate as direct write e-beam resist, sub-10 nm Ni lines have been fabricated.[24] While using a metal−organic precursor as a direct write resist, an additional advantage is that the patterned precursor can be transformed into a desired functional material[25] (besides metal), simply by appropriately choosing the thermolysis conditions. Working with metal−organic precursors, soft lithography methods such as micromolding in capillaries (MIMIC)[26] can also be an attractive possibility, especially for large-area patterning. A direct micromolding technique has been explored in the literature with various soluble functional material inks. For instance, Greco et al.[27] fabricated conductive Pt stripes using a Pt carbonyl cluster precursor. Using alkanethiolates, Pd[28] and its sulfide[25] patterns have been micromolded. Nevertheless, these precursors are specific to the material, and a general precursor for obtaining patterns of various materials was not addressed thus far. For the first time, we explored the possibility of using metal anion ToABr complexes as single-source precursors for metals, alloys, nitrides, oxides, and sulfides. In what follows, we first examine the ToABr-mediated transfer of metal anions across the aqueous organic interface,[29] to form metal anion−ToABr complexes, and then investigate the efficacy of the complexes as single-source precursors in e-beam lithography and micromolding methods under the chosen thermolysis conditions.

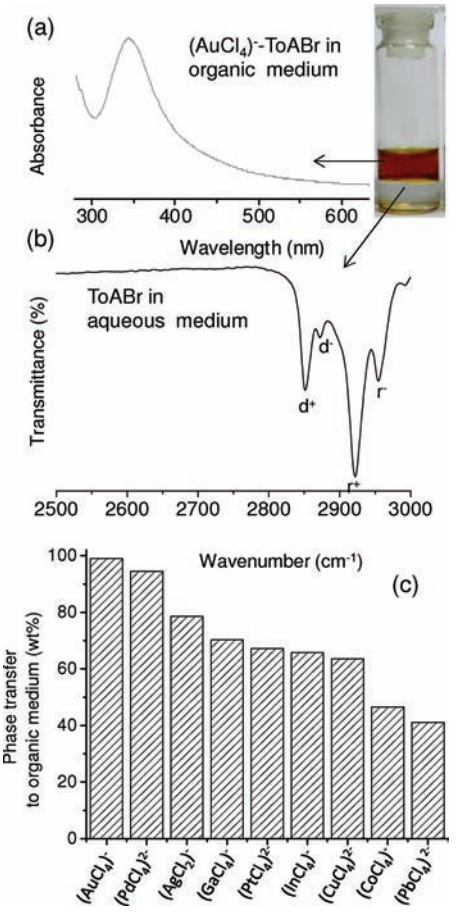

Figure 1. Aqueous−organic phase transfer of metal anions. (a) UV−visible absorption spectrum of the $(AuCl_4)^-$ phase transferred to ToABr (organic phase). A strong absorption band at 345 nm is characteristic of the MLCT band of the $(AuCl_4)^-$ complex. The LMCT band at lower wavelength (260 nm) is merged with the scattering from the glass. A photograph showing the biphasic mixture is given alongside. (b) FTIR spectrum of the ToABr which was transferred to the aqueous phase. ToABr in toluene was reacted with water, and the bottom aqueous solution was examined with FTIR. (c) Phase transfer efficiency of ToABr for various metal anions as estimated by gravimetry.

RESULTS AND DISCUSSION

Many metal anions such as $(AuCl_4)^-$ exhibit visible color due to metal-to-ligand charge transfer, which is often employed to monitor the process of transfer of the ions. Thus, the UV−visible spectrum shown in Figure 1a exhibits a peak at ∼345 nm corresponding to $(AuCl_4)^-$ ions[30] transferred to the organic phase. For ToABr, though the residence is organic medium, there may be some crosstalk at the interface effectively bringing a small fraction of ToABr into the aqueous medium as revealed using infrared spectroscopy (Figure 1b). This may adversely affect its transfer efficiency for metal anions. Among the examined cases (Figure 1c), the efficiency is highest for $(AuCl_4)^-$ (99%), $(PdCl_4)^{2-}$ being at 94.5%. The anions of Pt, Cu, Ga, and In are transferred by ToABr with efficiency in the range 60−70%. The transfer efficiency is poor for Co(46%) and Pb (41%). There may be many factors[31,32] which influence the process such as charge and size of the anion, pH of the aqueous chloroanion

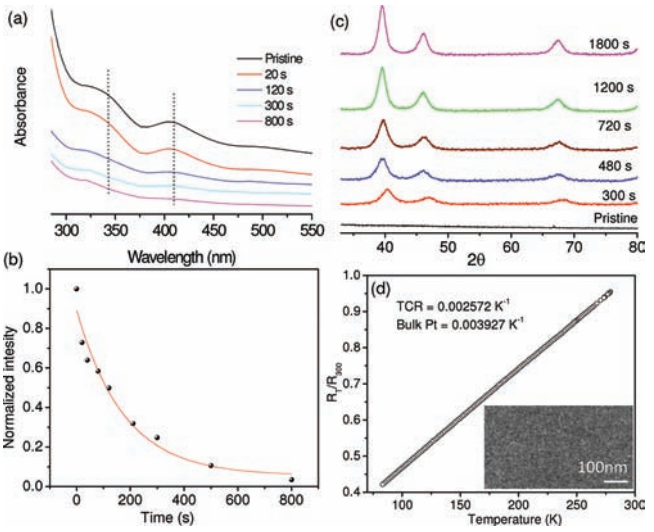

Figure 2. Metallization of Pt−ToABr. (a) UV−visible absorption spectra of Pt−ToABr film upon heating at 180 °C for various times as mentioned. (b) Intensity of the 342 nm band versus time of thermolysis and (c) XRDs of Pt formed by thermolysing Pt−ToABr film for various times at 250 °C (250 °C was chosen instead of 180 °C for better crystallinity). (d) Four-probe resistance measurement of the thermolyzed Pt nanocrystalline film with SEM image as inset.

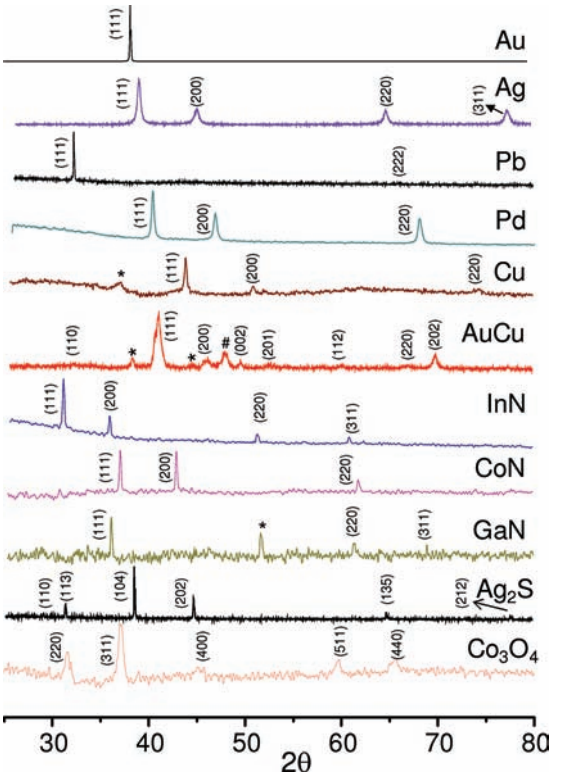

Figure 3. XRD data of the products. The peaks are indexed following JCPDS PDF files indicated in parentheses. Au (65-2870), Ag (89-3722), Pb (87-0663), Pd (88-2335), Cu (85-1326) (the peak marked * is due to Cu_2O; as Cu undergoes air oxidation rapidly, it may require encapsulation[35]), AuCu (89-2036) (the peaks marked * and # are due to Au and CuBr, respectively), InN (88-2365), CoN (83-0831), GaN (80-0011) (the peak marked * is due to a hexagonal GaN), Ag_2S (75-1061), and Co_3O_4 (65-3103).

solution, the organic solvent (toluene), etc. which we have not investigated in further detail in this study. Besides octyl, alkyl ammonium bromides of other chain lengths (butyl, decyl, and hexadecyl) have been tried out. The butyl complex is less soluble in toluene, while for decyl and hexadecyl, the anion transfer efficiencies were found to be poorer (Table S1, Supporting Information). The formed complexes with ToABr have many important attributes—they are air stable and can be solubilized repeatedly in low boiling point solvents such as toluene, ethanol, chloroform, etc., and the crystallization to the solid state is rapid.

The metal anion−ToABr interaction is completely electrostatic which should make the separation of metal from ToABr rather easy.[12] The process of metallization was carefully followed using UV−vis spectroscopy with Pt as an example. The phase transferred $(PtCl_4)^{2-}$−ToABr (Pt−ToABr for brevity) coated as a film on a glass slide shows two bands at 342 and 410 nm corresponding to the d−d transitions.[33] The spectra were recorded while heating the film at 180 °C for increasing duration, 20−800 s as shown in Figure 2a. The d−d bands diminish in intensity gradually and almost disappear after 800 s. The decrease in the intensity of the 340 nm band is exponential (Figure 2b) with a time constant of 175.9 s, indicating that the process is rather slow. In addition, XRD was used as a tool to monitor the metallization process (Figure 2c). The pristine Pt−ToABr film does not show any features in the range relevant for crystalline Pt. After thermolysing the film for 5 min, the appearance of small peaks is evident in the XRD data. With increasing time of thermolysis (Figure 2c), the XRD peaks corresponding to crystalline Pt grew in intensity, due to an overall improvement in the crystallinity. However, the peaks were broad as the diffracting regions were essentially nanoparticles. Using the Scherrer formula, the particle size was estimated to be ∼8 nm (see calculation in S1, Supporting Information). A corresponding SEM image shows that indeed the thermolyzed Pt film is composed of nanoparticles (see inset in Figure 2d and also TEM in Figure S2, Supporting Information). The EDS spectrum shows that the overall content of carbon present in the spectrum is ∼19 atom % (Figure S3b, Supporting Information), which is not unusual and indeed is relatively less compared to other results in the literature.[34] The metallization process (see TGA and FTIR in Figure S3, Supporting Information) gives us an idea that the ToABr ligand neatly desorbs around 250 °C to give rise to Pt metal. Four-probe resistivity data of the film were measured down to 77 K (Figure 2d). Room-temperature resistivity of the film is 350 $\mu\Omega\cdot$cm. This value, although higher compared to bulk Pt (10.5 $\mu\Omega\cdot$cm), is comparable to the Pt deposited by beam-induced depositions and is much lower than the previously reported data on Pt obtained from metal−organic precursor decomposition (see, for example, ref 27; the value is ∼28 901 $\mu\Omega\cdot$cm). The temperature coefficient of resistance, 0.00257 K^{-1}, is close to that of bulk Pt (0.00393 K^{-1}).

As many metals form anionic complexes which could be phase transferred to ToABr solutions (Figure 1c), we exploited them as single-source precursors for various nanomaterial products. The precursors were drop coated as thin films onto glass substrates and thermolyzed under controlled conditions. The XRD data are shown in Figure 3 and the various results in Table 1. While metals such as Au, Pt, and Pd could be obtained by thermolysis in air, Cu and Ag formed bromides (Figure S4, Supporting Information) which further required reduction using $NaBH_4$. Thermolysis in H_2 atmosphere at 375 °C appears to be most effective for producing

Table 1. M−ToABr Complexes As Single-Source Precursors to Various Nanomaterials under Controlled Thermolysis Conditions[a]

		thermolysis conditions							
no.	M−ToABr precursor (M)	temp (°C)	time (h)	atmosphere	material	morphology	particle size (nm)	property measured[b]	more details in Figure
1	Pt	250	1	air	Pt	particulates	5−10	• ρ = 350.2 $\mu\Omega$.cm • ρ/ρ° = 33.35	2 & S9a
2	Au	250	1	air	Au	particulates	5−40	crystallinity[#] and morphology	3 & 5k
3	Ag	250	1	air	Ag[*]	sheetlike	25−50	• ρ = 1840 $\mu\Omega$.cm • ρ/ρ° = 1159.4	S9e
4	Pb	375	1	H_2	Pb	densely packed particles	10−150	crystallinity and morphology	S9c
5	Pd	250	1	air	Pd	particulates	50−200	• ρ = 67.57 $\mu\Omega$.cm • ρ/ρ° = 6.41	S9b
6	Cu	375	1	N_2	Cu[*]	particulates	10−20	• ρ = 440 $\mu\Omega$.cm • ρ/ρ° = 262.2	S9d
7	Au:Cu = 1:1	375	3	N_2	AuCu	plates	400	tetragonal	S9f
8	In	375	3	N_2/Ar	InN	particulates	15−20	band gap ∼ 1.63 eV	S9i & S10
9	Co	375	3	Ar	CoN	cubic-shaped particles	10−200	• NaCl like structure • magnetic hysteresis • Cu electroless deposition	S9g, S11, S12
10	Ga	375	3	N_2/Ar	GaN	pyramid-shaped nanoparticulates	50−100	• cubic structure with some hexagonal impurity (marked by [*] in XRD)[#] • band gap ∼3.44 eV	3, S9h, S10
11	Ag (+C_{12}SH, = 1:5)	375	1	H_2	α-Ag_2S	particulates	30−200	monoclinic	S9j
12	Co	375	1	air/O_2	Co_3O_4	porous nanowalls	200	crystallinity and morphology	S9k
13	Zn	250	1	air	ZnO	particulates	5−20	Wurtzite structure	S17a

[a] The product morphology and functional properties as measured are also listed. [b] ρ = resistivity and ρ^o = bulk resistivity. [*] In these cases, metal bromides were obtained, to be reduced by $NaBH_4$. [#] See Figure 3 for XRD data of 2−12; 1 and 13 are shown in Figures 2 and 6, respectively.

crystalline Pb. For the formation of nitrides, Co, Ga, and In precursors were heated in N_2 or Ar atmosphere at 375 °C. While GaN and InN are important semiconductors, CoN finds application in electronic industry for Cu electroless deposition.[36] Treating in air or O_2, one may obtain oxide phases such as Co_3O_4. It is possible to prepare alloys as well, such as AuCu (see Table 1). By adding alkanethiol to the phase-transferred Ag−ToABr precursor and thermolysing in H_2, Ag_2S was also prepared.[37]

The ligand chosen, namely, ToABr, makes the metal highly processable. Figure 4 shows the Pt patterns obtained by direct micromolding and direct write EBL of the Pt−ToABr complex. For direct micromolding, a patterned PDMS stamp kept on a Si substrate was showered with ∼60 μL of toluene solution of Pt−ToABr while heating to 250 °C. The microchannels formed at the interface of the PDMS stamp and the substrate got filled with the solution due to capillary action (Figure 4a). After thermolysis for 30 min, the stamp was cooled to room temperature and removed to obtain Pt grating stripes of ∼1 μm wide and spacing ∼500 nm, in conformity with the stamp geometry. The stripes were continuous, without cracks, spread over large areas (Figure S5, Supporting Information). As revealed by the AFM image, the height of the μ-stripes was around ∼75 ± 5 nm (Figure 4b) with roughness of ∼1.5 nm. Figure 4c shows the SEM image of the stripes, revealing a smooth morphology. The EDS map in Figure 4d shows the presence of Pt only along the μ-stripes. The obtained stripes were well conducting.[38] A variety of substrates including flexible substrates (e.g., polyimide) can be used for patterning the Pt μ-stripes, the process temperature being low. Using nanoentrapment molding developed in the laboratory,[28] we were successful in patterning Pt nanowires (width, ∼70 nm) with this precursor (Figure S7, Supporting Information).

As mentioned earlier, direct write e-beam resist action is achievable with long-chain hydrocarbons.[19,39] Exploiting the sensitivity of the hydrocarbon chain (present in ToABr[40]) to the e-beam (see Figure S8, Supporting Information), it is possible to write assortment of Pt structures with direct write EBL (Figure 4e to j). After e-beam exposure, the loss of order among the alkane chains leads to insolubility of the exposed regions during

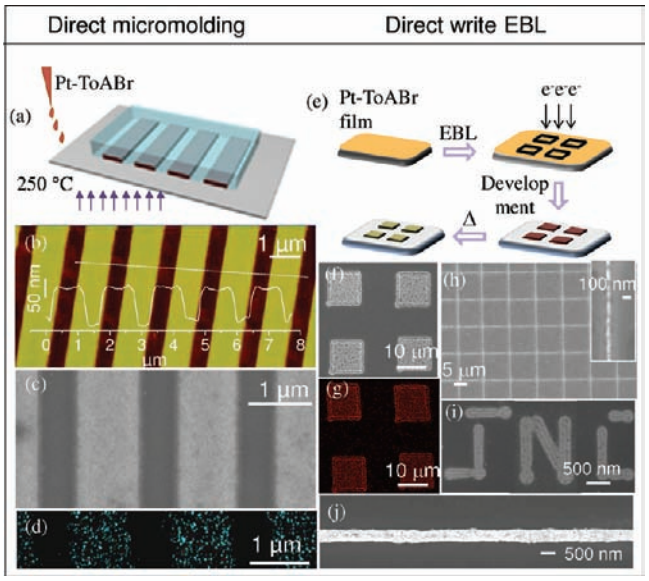

Figure 4. Pt patterning as an example. (a) Schematic showing the direct micromolding process. PDMS stamp hosting the microchannels is kept on a flat substrate, and the precursor solution is dropped along one edge, thus making it flow in the microchannels. The entire setup is heated to 250 °C at a ramp of 2 °C per min and held at 250 °C for 30 min. (b) AFM image of the formed Pt μ-stripes along with the z-profile along the dotted line. (c) SEM image showing the continuous stripes and (d) Pt M level EDS map of the stripes. (e) Schematic showing the direct write EBL process; precursor is spincoated on a substrate, exposed to e-beam in the desired pattern, developed in toluene for 5 s, and thermolyzed in air at 250 °C for 1 h. (f) and (g) are, respectively, the SEM images of the Pt squares and corresponding Pt M level EDS map. (h) A Pt mesh structure drawn with EBL, line width being ~60 nm. SEM images of (i) Pt alphabets and (j) long Pt nanowire drawn by EBL.

developing in a solvent (Figure S8, Supporting Information). Figure 4f and g shows the SEM and the corresponding EDS map of the Pt squares patterned by EBL with a 10 kV e-beam and dosage of ~800 μC/cm^2 (for SEM images of various products see Figure S9, Supporting Information). The e-dosage required here is much lower than the typical values reported for direct write precursors, e.g., 15 mC/cm^2 for ZnO[41] and 300 mC/cm^2 for Ni.[24] Figure 4h, i, and j has various examples of the Pt patterns revealing the continuity of the features written. The complexes listed in Table 1 have been subjected to direct micromolding as well as to direct write EBL. Flowing the precursor solution inside the microchannels, and thermolysing in a controlled atmosphere (same as mentioned for films), patterned μ-stripes of Pd, Pb, CoN, and Au were realized (see Figure 5a–d). The patterns are uniform over large areas—this is clearly evident in the inset of Figure 5b, which shows an optical micrograph, showing the colors split by patterned Pb μ-stripe grating due to diffraction from ambient light. Also, the morphology of the μ-stripes is composed of nanoparticles. The formed patterns being gratings, diffraction is an ideal macroscale tool for identifying the patterns. Figure 5e shows linear diffraction pattern formed by shining a red laser (~650 nm) onto a transmission grating of μ-stripes. Employing direct write EBL, diverse nanopatterns of various materials were created. Figure 5f shows a Cu nanowire, with smooth morphology even at higher magnifications. Figure 5g shows microsquares composed of Pd nanoparticles (see also Figure 5h) with mean size of ~12 nm (see histogram in Figure 5i). Direct write EBL of Au–ToABr (Figure 5j) produced relatively polydisperse Au nanoparticles (see Figure 5k) with mean size of ~20 nm (Figure 5l). Ag nanowire was formed by performing direct write EBL on Ag–ToABr film. After development and air thermolysis, AgBr nanowire was formed which was reduced by $NaBH_4$ to give rise to Ag nanowire. The roughness along the Ag nanowire edges came up during the reduction step (Figure 5m). Confocal images of the patterned InN squares, nanowires, and stripes on glass substrate are shown in Figure 5n and o. The emission is primarily in the red region. Dots of GaN ~ 100 nm wide formed by direct write EBL are shown in Figure 5p. A GaN circle patterned by direct write EBL shows green emission selectively from the patterned region in confocal image (Figure 5q). Further, the emission at different wavelengths examined by confocal imaging also emphasizes that the emission peak wavelengths for InN and GaN are at ~620 and ~540 nm, respectively (Figures S13 and S14, Supporting Information). Tiny dots of CoN examined by magnetic force microscopy (MFM) are shown in Figure 5r (see also Figure S15, Supporting Information). CoN nanoparticles show darker contrast (attractive force) with either magnetization of the AFM tip, indicative of the paramagnetic nature of the sample. Patterns of CoN written by direct write EBL show smooth line edges as shown in Figure 5s, t, and u.

The anion transfer efficiency by ToABr is a matter of concern with some metals, partly because suitable anions cannot be found. Instead, even simple salts can be tried out. In the case of $Zn(OAc)_2$, for instance, there was hardly any complex formation with ToABr in the organic phase; rather, ToABr was transferred from the organic to the aqueous phase. It is surprising that ToABr exhibits a definite interaction with $Zn(OAc)_2$ (see XRD in Figure S16, Supporting Information), although the latter is not an anionic complex. A thermolysis in air at 250 °C produced ZnO films (Figure 6a and Figure S17a, Supporting Information) as well as micro- and nanopatterns by micromolding and nanoentrapment molding, respectively (Figure 6b,c). ZnO is an important functional material in optical, electrical, piezoelectric, and optoelectronic applications,[42] and there are several reports on patterning ZnO.[43,44] For direct micromolding of ZnO, a polymer liquid precursor is known, but the recipe demands an additional step of high-temperature annealing.[45] Here, we took the advantage of ToABr functionality for making a viable precursor solution but in the aqueous medium. Patterned ZnO μ-stripes on the Si substrate are shown in Figure 6b. Importantly, the feature size could be further reduced, using the method of "nanoentrapment molding"[28] (for details, see Figure S5, Supporting Information). Thus, ~70 nm wide ZnO nanolines were formed (Figure 6c). Perhaps the aqueous route of phase transfer is extendable to other metals, which may not form anionic complexes readily.

For the ToABr-mediated route, though it works well for patterning a large number of materials, in certain cases such as Ag and Cu which form bromides following air thermolysis an additional process step of reduction is required. To overcome this limitation, we have tried other phase transfer agents, devoid of halides, such as dodecylamine (DDA).[46] DDA transfers metal ions by forming coordination complexes, and it works for almost all the metals, with transfer efficiencies of ~95%.[46] When Ag–DDA and Cu–DDA complexes were used as single-source precursors, crystalline metal films were obtained following thermolysis (Figure 6d; Figure S17b and c, Supporting Information). DDA being a semisolid at room temperature makes processing difficult. However, we were successful in micromolding the

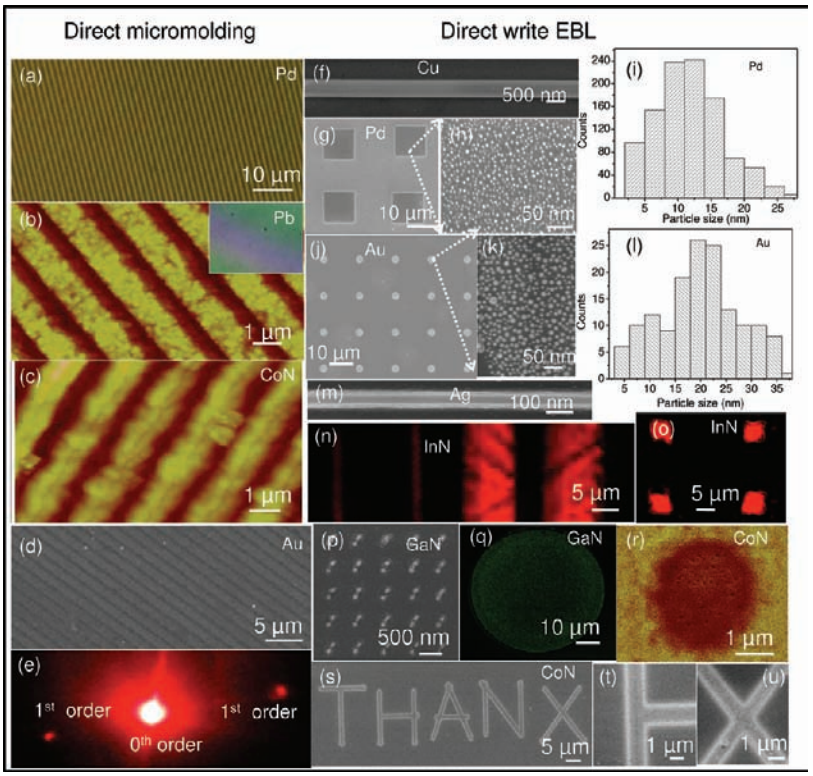

Figure 5. Various M−ToABr precursors subjected to patterning by direct micromolding (a−e) and direct write EBL (f−u). (a) Optical image of Pd μ-stripe grating and AFM images of Pb (b) and CoN μ-stripe gratings (c). (d) SEM image of Au μ-stripe grating and (e) optical diffraction pattern from the grating. SEM images of (f) Cu nanowire, (g, j) Pd and Au nanoparticle patterns with magnified views as indicated by arrows in (h, k) and histograms in (i, l), respectively, and (m) Ag nanowire. (n, o) Confocal images of the InN EBL patterns. (p) SEM image of GaN dots. (q) Confocal image of patterned GaN circle. (r) MFM image of CoN. (s) SEM image of EBL patterns of CoN with magnified views in (t) and (u).

precursors to obtain well-defined patterns (Figure 6e and f). Although the precursor responded to e-beam, the roughness of the spin-coated film (~30−50 nm) was prohibitive for further processing (Figure S18, Supporting Information).

■ CONCLUSION

From the above observations, it is evident that metal anions complexed with tetraoctylammonium bromide could serve as single-source precursors for thin nanocrystalline films of most metals, alloys, nitrides, oxides, and sulfides involving a single process step, namely, thermolysis in a controlled atmosphere. Thin precursor films coated on a substrate serve as e-beam resists for direct writing due to extreme e-beam sensitivity of the hydrocarbon chain. Instead of coating on a substrate, the precursor solutions may be flowed into micromold capillaries to produce patterns of the desired material, covering large areas. This generic approach should be extendable to materials not explored in this study.

■ MATERIALS AND METHODS

All metal salts (see Supporting Information) and tetraoctylammonium bromide (ToABr) were obtained from Sigma Aldrich, and dodecylamine (DDA) was purchased from Merck. They were used without further purification. The water used throughout this investigation was double distilled and deionized. To 50 mM aqueous metal solution was added 50 mM ToABr. In some cases, conc. HCl was used to aid the formation of metal anions (details for individual anions are reported in Supporting Information). The gravimetry for M−ToABr (M = metal) was done by taking metal salt solution (for example $HAuCl_4$ as the mother liquor) and the aqueous phase left after phase transferring with ToABr. Approximately 100 μL of solution of both mother liquor and aqueous phase was coated on preweighed coverslips and thermolyzed at 100 °C for 1 h. After cooling to room temperature, the coverslip was weighed again, and from the weight difference, the amount of metal which did not phase transfer was calculated. UV−visible spectra were recorded using a Perkin−Elmer Lambda 900 UV/vis/near-IR spectrophotometer. Fourier transform infrared measurements were done using a Bruker IFS66v/s spectrometer with a resolution of 2 cm^{-1}. X-ray diffraction (XRD) measurements were performed using a Siemens Seifert 3000TT diffractometer (Cu Kα 1.5406 Å, scan rate, 0.5 min^{-1}). EBL was performed using a Nova NanoSEM 600 instrument (FEI Co., The Netherlands). The EDS mapping was performed at 10 kV (energy window, 10 eV) with a beam current of 1.1 nA, the dwell time per pixel being 30 s. AFM imaging was performed with a Digital Instruments Multimode head attached to a Nanoscope-IV controller (Veeco, USA). The MFM tip (CoCr-coated Si) was magnetized vertically along the tip axis, thereby allowing detection of the perpendicular component of the stray field emanating from the sample surface with a spatial resolution of ≈50 nm. Thickness measurements were performed using a Stylus profiler Dektak 6 M (Veeco, USA). The laser used for diffraction measurement is a diode laser of 650 nm wavelength. The optical images were procured with the microscope of Laben, India. Four-probe, low-temperature resistivity measurements were done using examina probe cooling/heating stage (Linkam,UK). The confocal images were recorded using a Zeiss LSM 510 laser scanning confocal microscope.

Direct Write EBL and Direct Micromolding. Si(100) substrates (n-doped, 4−7 Ω·cm) and glass substrates were cleaned by

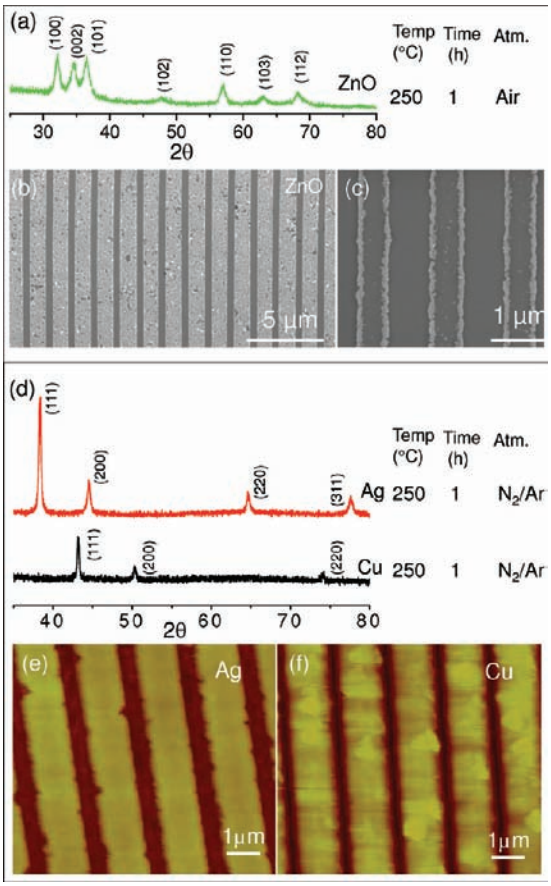

Figure 6. Alternate routes. (a) XRD pattern of ZnO (JCPDS 89-1397) film formed by thermolysing the aqueous precursor and SEM image of patterned ZnO in μ-stripes (b) and nanolines (c). (d) XRD patterns of Ag and Cu films formed by thermolysis of Ag−DDA and Cu−DDA complexes with the corresponding planes indexed according to the JCPDS PDF files: Ag (89-3722) and Cu (85-1326). Thermolysis conditions are mentioned. AFM images of (e) Ag and (f) Cu μ-stripes formed by direct micromolding of Ag−DDA and Cu−DDA complexes, respectively, followed by thermolysis in an inert atmosphere.

ultrasonicating in acetone and double distilled water and dried under flowing N_2. The e-resist film was made by spin coating of the M−ToABr solution at 2000 rpm for 1 min. EBL was performed using a Nova NanoSEM 600 instrument (FEI Co., The Netherlands). The electron beam energy employed for patterning was 5 kV (for Pt−ToABr, 10 kV). For direct micromolding, elastomeric stamps were fabricated by replica molding of PDMS on a commercially available compact disk (Sony CD-R). PDMS was prepared by mixing Sylgard 184 curing agent (Dow Corning) and its elastomer in the ratio of 1:10 by weight. After degassing the mixture under vacuum for 30 min, PDMS was poured onto the polycarbonate backing of the master (CD) and then cured in the oven at 60 °C overnight. The stamp peeled off from the master contained protruding line features of ~505 nm width separated by ~950 nm channels. The stamp's thickness was ~2 mm, with its weight being ~2.4 g. Cured PDMS stamps were cleaned using hexane and further ultrasonicated in ethanol to remove any low-molecular-weight, uncured oligomers. After keeping the PDMS stamp on the substrate, ~60 μL of the M−ToABr precursor solution is injected at the interface of the stamp and the substrate using a micropipet. The entire setup was heated to 250 °C. To pattern metal nanowires via modified micromolding,[28] a pressure of ~1000 Pa was applied on top of the PDMS by placing an appropriate weight while micromolding.

■ ASSOCIATED CONTENT

Supporting Information. The contents of Supporting Information include the following: (1) detailed materials and methods, (2) Table S1 for phase transfer efficiencies with various quaternary alkylammonium bromides, (3) calculation of Pt particle size, (4) TEM image of Pt nanoparticles, (5) TGA, EDS, and FTIR of thermolyzed Pt nanocrystalline film, (6) XRDs of CuBr and AgBr, (7) SEM images of the Pt μ-stripes over large areas, (8) $I-V$ characteristics and optical micrograph of Pt μ-stripes, (9) SEM images of Pt fine lines by nanoentrapment molding, (10) FTIR spectra of the precursor film before and after exposure to e-beam, (11) SEM images of thermolyzed films of various nanomaterials, (12) band gap calculation of InN and GaN, (13) magnetic measurements of CoN film, (14) SEM, XRD, and EDS of CoN film electrolessly deposited with Cu, (15) confocal wavelength scan of InN and GaN patterns, (16) MFM images of CoN, (17) XRD of Zn−ToABr, (18) SEM images of ZnO, Ag, and Cu thermolyzed films. This material is available free of charge via the Internet at http://pubs.acs.org.

■ AUTHOR INFORMATION

Corresponding Author
kulkarni@jncasr.ac.in

■ ACKNOWLEDGMENT

The authors thank Prof. C. N. R. Rao for his constant encouragement. We thank Professor A. Sundaresan and Mr. Nitesh for help in magnetic measurements. We thank Dr. Basavaraja S, VINL, for help in AFM measurements. Support from the Department of Science and Technology, India, is gratefully acknowledged. Radha B thanks CSIR, India, for a fellowship.

■ REFERENCES

(1) (a) Fischer, R.; Scherer, W.; Kleine, M. *Angew. Chem., Int. Ed.* **1993**, *32*, 748. (b) Maury, F. *J. Phys. IV* **1995**, *5*, 449–463.
(2) Lange, F. F. *Science* **1996**, *273*, 903–909.
(3) Chrisey, D. B. *Science* **2000**, *289*, 879–881.
(4) Piner, R. D.; Zhu, J.; Xu, F.; Hong, S.; Mirkin, C. A. *Science* **1999**, *283*, 661–663.
(5) Weiss, D. N.; Meyers, S. T.; Keszler, D. A. *J. Vac. Sci. Technol., B* **2010**, *28*, 823–828.
(6) Malik, M. A.; O'Brien, P. In *Precursor Chemistry of Advanced Materials*; Fischer, R. A., Ed.; Springer: Berlin/Heidelberg, 2005; Vol. 9, pp 173−204.
(7) Banger, K. K.; Yamashita, Y.; Mori, K.; Peterson, R. L.; Leedham, T.; Rickard, J.; Sirringhaus, H. *Nat. Mater.* **2010**, *10*, 45–50.
(8) Sardar, K.; Dan, M.; Schwenzer, B.; Rao, C. N. R. *J. Mater. Chem.* **2005**, *15*, 2175–2177.
(9) Park, J.; An, K.; Hwang, Y.; Park, J.-G.; Noh, H.-J.; Kim, J.-Y.; Park, J.-H.; Hwang, N.-M.; Hyeon, T. *Nat. Mater.* **2004**, *3*, 891–895.
(10) Belova, V.; Khol'kin, A.; Zhidkova, T. *Theor. Found. Chem. Eng.* **2007**, *41*, 743–751.
(11) Park, Y. J.; Fray, D. J. *J. Hazard. Mater.* **2009**, *164*, 1152–1158.
(12) Brust, M.; Walker, M.; Bethell, D.; Schiffrin, D. J.; Whyman, R. *J. Chem. Soc., Chem. Commun.* **1994**, *7*, 801–802.
(13) Castro, E. G.; Salvatierra, R. V.; Schreiner, W. H.; Oliveira, M. M.; Zarbin, A. J. G. *Chem. Mater.* **2010**, *22*, 360–370.
(14) Coronado, E.; Ribera, A.; García-Martínez, J.; Linares, N.; Liz-Marzán, L. M. *J. Mater. Chem.* **2008**, *18*, 5682–5688.
(15) Goulet, P. J. G.; Lennox, R. B. *J. Am. Chem. Soc.* **2010**, *132*, 9582–9584.

(16) Ibañez, F. J.; Zamborini, F. P. *ACS Nano* **2008**, *2*, 1543–1552.
(17) In addition, using the Au anionic complex with ToABr as a CVD precursor, there have been attempts to deposit Au nanoparticles by thermolysis at elevated temperatures: Palgrave, R. G.; Parkin, I. P. *Gold Bull.* **2008**, *41*, 66–69.
(18) Xia, Y.; Xiong, Y.; Lim, B.; Skrabalak, S. E. *Angew. Chem., Int. Ed.* **2009**, *48*, 60–103.
(19) Bhuvana, T.; Kulkarni, G. U. *ACS Nano* **2008**, *2*, 457–462.
(20) Nakamoto, M.; Yamamoto, M.; Fukusumi, M. *Chem. Commun.* **2002**, *15*, 1622–1623.
(21) Werts, M. H. V.; Lambert, M.; Bourgoin, J. P.; Brust, M. *Nano Lett.* **2002**, *2*, 43–47.
(22) Reetz, M. T.; Winter, M.; Dumpich, G.; Lohau, J.; Friedrichowski, S. *J. Am. Chem. Soc.* **1997**, *119*, 4539–4540.
(23) Corbierre, M. K.; Beerens, J.; Lennox, R. B. *Chem. Mater.* **2005**, *17*, 5774–5779.
(24) Nedelcu, M.; Saifullah, M. S. M.; Hasko, D. G.; Jang, A.; Anderson, D.; Huck, W. T. S.; Jones, G. A. C.; Welland, M. E.; Kang, D. J.; Steiner, U. *Adv. Funct. Mater.* **2010**, *20*, 2317–2323.
(25) Radha, B.; Kulkarni, G. U. *Adv. Funct. Mater.* **2010**, *20*, 879–884.
(26) Kim, E.; Xia, Y.; Whitesides, G. M. *Nature* **1995**, *376*, 581–584.
(27) Greco, P.; Cavallini, M.; Stoliar, P.; Quiroga, S. D.; Dutta, S.; Zacchini, S.; Iapalucci, M. C.; Morandi, V.; Milita, S.; Merli, P. G.; Biscarini, F. *J. Am. Chem. Soc.* **2008**, *130*, 1177–1182.
(28) Radha, B.; Kulkarni, G. U. *Small* **2009**, *5*, 2271–2275.
(29) For similar studies in the literature with regard to other phase transfer reagents, please refer to: Yang, J.; Sargent, E.; Kelley, S.; Ying, J. Y. *Nat. Mater.* **2009**, *8*, 683–689. Prakash, A.; Zhu, H.; Jones, C. J.; Benoit, D. N.; Ellsworth, A. Z.; Bryant, E. L.; Colvin, V. L. . *ACS Nano* **2009**, *3*, 2139–2146.
(30) Isaacs, S. R.; Cutler, E. C.; Park, J. S.; Lee, T. R.; Shon, Y. S. *Langmuir* **2005**, *21*, 5689–5692.
(31) Mooiman, M. B. *Precious Met.* **1993**, *17*, 411–434.
(32) Kondo, K.; Ourachi, T.; Kaneiwa, T.; Matsumoto, M. *Solvent Extr. Res. Dev., Jpn.* **2000**, *7*, 176–184.
(33) Cox, L. E.; Peters, D. G. *Inorg. Chem.* **1970**, *9*, 1927–1930.
(34) The amount of carbon in the deposited Pt for ion- and electron beam-induced processes can vary in the range from 40 to 55% and 60 to 75% according: Langford, R. M.; Wang, T. X.; Ozkaya, D. *Microelectron. Eng.* **2007**, *84*, 784–788. For instance, in the following, 66% carbon is left behind in the Pt deposit:Telari, K. A.; Rogers, B. R.; Fang, H.; Shen, L.; Weller, R. A.; Braski, D. N. *J. Vac. Sci. Technol., B* **2002**, *20*, 590–595.
(35) Gardner, D. S.; Onuki, J.; Kudoo, K.; Misawa, Y.; Vu, Q. T. *Thin Solid Films* **1995**, *262*, 104–119.
(36) WO/2009/088522, United States, 2009.
(37) In contrast to literature reports which make use of additional sulfiding agents, Na_2S, here thermolysing in H_2 lead to the sulfidic phase: Schaaff, T. G.; Rodinone, A. J. *J. Phys. Chem. B* **2003**, *107*, 10416–10422. Without either of the two mentioned, a simple air treatment will yield Ag nanoparticles:Carotenuto, G.; Martorana, B.; Perlo, P.; Nicolais, L. *J. Mater. Chem.* **2003**, *13*, 2927–2930.
(38) From the stripes molded onto a glass substrate, the resistivity of each Pt stripe is found to be 540 $\mu\Omega\cdot$cm (see Supporting Information Figure S6). This value is somewhat higher than that obtained for the thin film of Pt (350 $\mu\Omega\cdot$cm). While being molded, the precursor decomposition might not be complete, owing to the confined environment in the microchannel, leaving a higher percentage of carbon (~40%) in the stripes. A rather simple step of air heating to 400 °C for 30 min brought down the carbon in the stripes to <5% with resistivity dropping to 281 $\mu\Omega\cdot$cm.
(39) In general, the solubility contrast of the resist that is seen during the developing process may arise due to the defects or the cross-linking of the chains following e dosage.
(40) We have found that neat ToABr is also a good e-beam resist.
(41) Saifullah, M. S. M.; Subramanian, K. R. V.; Kang, D. J.; Anderson, D.; Huck, W. T. S.; Jones, G. A. C.; Welland, M. E. *Adv. Mater.* **2005**, *17*, 1757–1761.
(42) Wang, Z. L. *J. Phys.: Condens. Matter* **2004**, *16*, R829–R858.
(43) Donthu, S.; Pan, Z.; Myers, B.; Shekhawat, G.; Xu, N.; Dravid, V. *Nano Lett.* **2005**, *5*, 1710–1715.
(44) Auzelyte1, V.; Sigg1, H.; Schmitt, B.; Solak, H. H. *Nanotechnology* **2010**, *21*, 215302–215308.
(45) Gobel, O. F.; Blank, D. H. A.; Elshof, J. E. T. *ACS Appl. Mater. Interface* **2010**, *2*, 536–543.
(46) Yang, J.; Sargent, E.; Kelley, S.; Ying, J. Y. *Nat. Mater.* **2009**, *8*, 683–689.